

Conduction-Based Modeling of the Biofilm Anode of a Microbial Fuel Cell

Andrew Kato Marcus, César I. Torres, Bruce E. Rittmann

Center for Environmental Biotechnology, Biodesign Institute at Arizona State University, 1001 South McAllister Avenue, P.O. Box 875701, Tempe, Arizona 85287-5701; telephone: 1-480-727-0848; fax: 1-480-727-0889; e-mail: andrew_marcus@asu.edu

Received 11 April 2007; revision received 28 May 2007; accepted 29 May 2007

Published online 14 June 2007 in Wiley InterScience (www.interscience.wiley.com). DOI 10.1002/bit.21533

ABSTRACT: The biofilm of a microbial fuel cell (MFC) experiences biofilm-related (growth and mass transport) and electrochemical (electron conduction and charger-transfer) processes. We developed a dynamic, one-dimensional, multi-species model for the biofilm in three steps. First, we formulated the biofilm on the anode as a “biofilm anode” with the following two properties: (1) The biofilm has a conductive solid matrix characterized by the biofilm conductivity (κ_{bio}). (2) The biofilm matrix accepts electrons from biofilm bacteria and conducts the electrons to the anode. Second, we derived the Nernst-Monod expression to describe the rate of electron-donor (ED) oxidation. Third, we linked these components using the principles of mass balance and Ohm’s law. We then solved the model to study dual limitation in biofilm by the ED concentration and local potential. Our model illustrates that κ_{bio} strongly influences the ED and current fluxes, the type of limitation in biofilm, and the biomass distribution. A larger κ_{bio} increases the ED and current fluxes, and, consequently, the ED mass-transfer resistance becomes significant. A significant gradient in ED concentration, local potential, or both can develop in the biofilm anode, and the biomass actively respire only where ED concentration and local potential are high. When κ_{bio} is relatively large (i.e., $\geq 10^{-3} \text{ mS cm}^{-1}$), active biomass can persist up to tens of micrometers away from the anode. Increases in biofilm thickness and accumulation of inert biomass accentuate dual limitation and reduce the current density. These limitations can be alleviated with increases in the specific detachment rate and biofilm density.

Biotechnol. Bioeng. 2007;98: 1171–1182.

© 2007 Wiley Periodicals, Inc.

KEYWORDS: anodic electron acceptor; biofilm anode; biofilm conductivity; conduction-based modeling; detachment; microbial fuel cell

Introduction

A microbial fuel cell (MFC) is a hybrid of biological and electrochemical reactors. The dualistic nature offers great promise for generating renewable energy, but it forces researchers to confront diverse scientific and engineering challenges. On the one hand, an MFC takes advantage of a feature common to microbiological systems: being able to utilize a wide range of organic and inorganic compounds as electron donor (ED) or fuel. Furthermore, a MFC exploits the value of electrochemical cells by directly generating electricity that can be conveniently used. On the other hand, research and development of MFCs demands interdisciplinary concepts and techniques from microbiology, environmental biotechnology, electrochemistry, electrical engineering, and material science. To harvest the benefits of MFCs, improvements to the current and power densities are required. Systematic understanding of the biological and electrochemical factors that control the performance of an MFC is needed to have improvements.

A major scientific challenge in MFC research is to understand the many biological and electrochemical phenomena that drive the oxidation of the fuel in the anode. Mathematical models for biofilm are useful in understanding and designing biofilm reactors having complex inter-related phenomena (Wanner et al., 2006). Model formulation is initiated by identifying key components and the parameters that represent them. Then, appropriate mathematical relationships are used to describe processes that affect the component parameters. Finally, the overall system is described by incorporating process expressions into mass-balance relationships for the components. Thus, the development of a mathematical model requires identifying key components, parameters, and processes.

Correspondence to: A. Kato Marcus
Contract grant sponsor: NASA
Contract grant number: 0720350C4441194
Contract grant sponsor: NZ Legacy
Contract grant sponsor: OpenCEL

 WILEY
InterScience®
DISCOVER SOMETHING GREAT

The biofilm on the anode of an MFC has at least three essential components: the ED substrate, the bacteria active in oxidizing the ED, and the electrons (e^-) removed in the oxidation and transferred to the anode. Three variables representing the components are the concentration of the ED, the accumulation of the biomass on the anode, and the electrical potential. Crucial features of the components in the MFC setting are:

- The magnitude of the anodic current increases in response to an increase in the ED concentration, usually following a saturation-type behavior (Gil et al., 2003; Kim et al., 2003; Liu and Logan, 2004).
- In electrochemistry, the anodic current depends on the amount of catalyst per unit surface area (i.e., the catalyst loading). In an MFC, the anodic current increases with the amount of biomass attached to the electrode (Bond et al., 2002; Reguera et al., 2006).
- In an electrochemical cell, the rate of electron-transfer to an electrode is controlled by the electrical potential, which can be viewed analogously to an “electron activity” that allows a chemical species to gain or lose an electron (Wang, 2000). The qualitative relationship between the current and electrical potential in an MFC is well established: an increase in the electrical potential of the anode increases the anodic current from the oxidation of ED until a plateau is reached (Liu et al., 2005; Liu and Logan, 2004; Ter Heijne et al., 2006).

These features suggest that the rate of ED oxidation in an anode biofilm can be represented by a multiplicative, dual-limitation relationship that involves the ED concentration and the electrical potential. This is analogous to the classical dual-limitation model, in which the rate of ED utilization is controlled by the concentrations of the ED and the electron acceptor (EA) (Wanner et al., 2006). Qualitatively, the electrical potential of the anode is analogous to the EA concentration, and the anode acts like an EA by accepting electrons from the bacteria.

Two mechanisms for transfer of electrons from the bacteria to the anode are recognized in the literature: electron shuttles (Rabaey et al., 2005) and conduction (Reguera et al., 2006). In the electron-shuttle mechanism, the electrons are transferred from bacterial cells to a soluble EA (i.e., the shuttle, also known as a mediator). The reduced shuttle diffuses to the anode, discharges its electrons, and then diffuses back to the bacterial cells to repeat the process. Thus, the EA is soluble and “shuttles” by diffusion. Shuttles can be supplied exogenously (e.g., neutral red), or bacteria in the anode compartment can produce endogenous electron shuttles, such as pyocyanin (Rabaey et al., 2005). Zhang and Halme (1995) developed a model for a batch MFC with exogenous shuttles, and they indicated that a high concentration of shuttles is essential for generating a high current. Although their model is for cell suspensions and not biofilm, their observation is consistent with conventional electrochemistry, which states that the current from an

electrode generally increases with the concentration of electroactive species (Wang, 2000).

In contrast to the conventional electrochemistry, MFCs are known to work efficiently under conditions that prohibit high concentrations of endogenous shuttles. For example, an MFC with a short hydraulic retention time of 2.5 h completely removed the original ED with 70% Coulombic yield (Lee et al., 2003), even though electron shuttles (if any were produced) would have been washed out. Also, current was recovered immediately upon medium replacement (and total loss of soluble shuttles) in a semi-batch MFC (Bond and Lovley, 2003; Holmes et al., 2004; Kim et al., 2004). These results suggest that the conduction mechanisms are dominant in many MFCs, especially in those with liquid flow.

In the conduction mechanism, bacteria transfer electrons to the anode from their membrane-bound electron carriers to the electrode via conductive materials in the biofilm matrix. Biofilm is known to accumulate biomass-derived solids that are not active biomass: in particular, extracellular polymeric substances (EPS) and inert (residual) biomass (Laspidou and Rittmann, 2004), and the accumulation of the conductive matrix seems to be essential for a continuous-flow MFC. Proteins are predominant components of EPS in many engineered biofilm systems (Dignac et al., 1998; Nielsen et al., 1997), and certain proteins appear to enhance the conductive properties of the biofilm matrix (Gorby et al., 2006; Reguera et al., 2006). Being conductive, the biofilm matrix is part of the anode, creating what we call the “biofilm anode.”

The matrix of EPS of at least some anode-respiring biofilms contains highly conductive nanowires that extend for tens of micrometers (Gorby et al., 2006; Reguera et al., 2006). In the EPS matrix of *Shewanella oneidensis* MR-1 that contained conductive nanowires, Gorby et al. (personal communication), confirmed the presence of cytochrome c by mass spectroscopy and antibody staining. In contrast, mutant strains of *S. oneidensis* MR-1, Δ MTRC/OMCA (deficient in decaheme c-type cytochromes MtrC and OmcA), and GspD (deficient in type-II secretion system in *Shewanella* required for the translocation of a 91-kDa c-type cytochrome), produced appendages similar in physical dimensions to the conductive nanowires but were significantly less conductive (Gorby et al., 2006). Furthermore, an anode biofilm of *G. sulfurreducens* had active biomass throughout its depth of 40–50 μ m and produced current about 10 times greater than pilA-gene deficient *G. sulfurreducens* (Reguera et al., 2006). These findings suggest that conductive appendages facilitate anode respiration by bacteria by conducting electrons.

In general, electron conduction is driven by a gradient of electrical potential; however, quantitative understanding between the rate that electrons conduct in a biofilm matrix and the electrical potential has not been established. Hence, the primary aim of this article is to develop a numerical model for a biofilm anode in which the conduction of electrons in the biofilm matrix is the mode of electron

transport from a bacterium to the anode. We take a similar approach to that of Bernardi and Verbrugge (1991, 1992), who first described a gas-diffusion electrode of a conventional fuel cell (1991) before they moved on to describe the entire fuel cell (1992). Hence, we examine the current density from the anode in this article and reserve the discussion of power density (which depends on the entire fuel cell) for future studies. We use the model to analyze the biofilm anode in the context of dual-limitation scenario that can be accentuated when two potentially conflicting objectives must be achieved with an MFC: high efficiency removal of the ED and a high rate of electrical energy generation.

Model Formulation

Our model for the biofilm anode is dynamic, one-dimensional, and multi-species. The biofilm grows along the z-axis perpendicular to the anode surface. The biofilm-anode interface is located at $z = 0$, and the biofilm thickness is L_f (cm). The biofilm consists of active and inactive biomass that develop naturally into “fuzzy layers” (Kissel et al., 1984; Rittmann and Manem, 1992; Wanner and Gujer, 1986); thus, the active and inert biomass compete for space.

We make the following four assumptions.

1. The biofilm matrix is a conductor characterized by the biofilm conductivity, κ_{bio} (mS cm^{-1}). At this stage, we assume that the active and inert biomass shares the same biofilm conductivity, but separate conductivity can be implemented later.
2. The active biomass transfers electrons to the conductive biofilm matrix as its only outlet for electrons generated in substrate and endogenous respirations. In the presence of other types of biomass and EAs, this assumption can be relaxed within the framework of multi-species model (e.g., Wanner and Gujer, 1986).
3. The rate of donor-substrate utilization depends on the local concentration of the donor (S_d) and the local potential (η).
4. The biofilm is well connected to the electrode. The charge-transfer reaction from the conductive biofilm matrix to the anode has negligible over-potential (or resistance).
5. A non-limiting flow of anions and cations in the biofilm maintains electroneutrality; thus, ions move with no ohmic loss.
6. The system is well buffered, and the pH change in the biofilm is negligible. This assumption can be relaxed later.
7. The transfer of electron from the bacteria to the conductive biofilm matrix is rapid and reversible; hence, we describe the electron-transfer at the interface (Eq. (2) in the next section) as a Nernstian system (Bard and Faulkner, 2001). The reversible electrochemistry of electron transport chain components (e.g., cyto-

chrome c) was established decades ago (Eddowes and Hill, 1977; Yeh and Kuwana, 1977).

Based on these assumptions, we formulate the model in the following sequence. First, we derive the Nernst-Monod expression—a quantitative expression that describes the relationship between the rate of ED utilization and two variables: ED concentration and electrical potential. Next, we link the rate expression with the biofilm anode processes (e.g., conduction) based on four principles: (1) a steady-state ED mass balance, (2) a steady-state electron balance, (3) Ohm’s law, and (4) a dynamic biomass mass balance. Finally, we derive a fundamental equation to describe the minimum potential required to sustain a steady-state biofilm.

Rates Of Substrate Utilization And Respiration

Bae and Rittmann (1996a,b) systematically and quantitatively established the multiplicative Monod model for dual donor–acceptor when both substrates are soluble:

$$q = q_{\text{max}} \phi_a \frac{S_d}{S_d + K_{S_d}} \frac{S_a}{S_a + K_{S_a}} \quad (1)$$

where

q = specific rate of ED utilization ($\text{mmol-ED mg}^{-1} \text{VS}^{-1} \text{day}^{-1}$; VS = volatile solids, a measure of biomass)

S_d = ED concentration (mmol-ED cm^{-3})

K_{S_d} = half-max-rate ED concentration (mmol-ED cm^{-3})

S_a = EA concentration (mmol-EA cm^{-3})

K_{S_a} = half-max-rate EA concentration (mmol-EA cm^{-3})

ϕ_a = volumetric fraction of active biomass (dimensionless)

q_{max} = maximum specific rate of ED utilization ($\text{mmol-ED mg-VS}^{-1} \text{day}^{-1}$)

The donor part of Eq. (1) ($S_d/S_d + K_{S_d}$) is retained from normal biofilm modeling because the Monod expression captures the kinetics of soluble substrates. However, the biofilm anode is not soluble, has no concentration, is not oxidized or reduced, and is a solid conductor that allows electrons to pass in response to the electrical-potential gradient. Thus, we refer to the anode and the biofilm anode as an “anodic electron acceptor” to distinguish it from a traditional soluble EA. We relate the potential of the anodic EA (E_{anode}) to the concentration of EA using the Nernst equation (Stumm and Morgan, 1996):

$$E_{\text{anode}} = E_A^0 - \frac{RT}{nF} \ln \left(\frac{S_a^0}{S_a} \right) \quad (2)$$

where

S_a^0 = a standard anodic-EA concentration ($1 \text{ mmol-EA cm}^{-3}$)

E_A^0 = standard reduction potential for the anodic EA (V)
 R = ideal gas constant (8.3145 J mol⁻¹ K⁻¹)
 F = Faraday constant (96,485 Coulomb per mol-e⁻)
 T = temperature (298.15 K)
 n = number of electrons transferred to the anodic EA

Since an electron is the component that passes through the biofilm anode, we set $n = 1$ by convention. We define E_{K_A} as the potential that occurs when $S_a = K_{S_a}$ (in Eq. (1)) and the rate is 1/2 the maximum rate:

$$E_{K_A} = E_A^0 - \frac{RT}{F} \ln\left(\frac{S_a^0}{K_{S_a}}\right) \quad (3)$$

Thus, E_{K_A} is the anodic acceptor potential for the half-maximum-rate. Substituting Eqs. (2) and (3) into Eq. (1), we obtain:

$$q = q_{\max} \phi_a \times \left(\frac{S_d}{S_d + K_{S_d}}\right) \frac{\exp\left(\frac{F}{RT}(E_{\text{anode}} - E_A^0)\right)}{\exp\left(\frac{F}{RT}(E_{K_A} - E_A^0)\right) + \exp\left(\frac{F}{RT}(E_{\text{anode}} - E_A^0)\right)} \quad (4)$$

We define the local potential as $\eta = (E_{\text{anode}} - E_{K_A})$ and simplify Eq. (4) to

$$q = q_{\max} \phi_a \left(\frac{S_d}{S_d + K_{S_d}}\right) \left(\frac{1}{1 + \exp\left[-\frac{F}{RT}\eta\right]}\right) \quad (5)$$

We refer to the last term in the parenthesis as the Nernst-Monod term, for which E_{K_A} is analogous to K_{S_a} . When $E_{K_A} = E_{\text{anode}}$, $\eta = 0$. Then, the exponential term equals 1, and the Nernst-Monod term gives one-half the maximum rate. Furthermore, to simplify the discussion of our model development, we define $E_{K_A} \equiv 0$; therefore, $\eta = E_{\text{anode}}$. The Nernst-Monod term shows that the rate of substrate utilization increases as the local potential increases until a plateau is reached. When the local potential is sufficiently high, the anodic EA saturates and donor oxidation limits the rate of substrate utilization.

The biofilm anode conducts electrons generated in endogenous respiration in the same manner as electrons generated from ED oxidation. Thus, the specific rate of endogenous respiration (r_{res} ; day⁻¹) is described using the same Nernst-Monod term:

$$r_{\text{res}} = b_{\text{res}} \phi_a \left(\frac{1}{1 + \exp\left[-\frac{F}{RT}\eta\right]}\right) \quad (6)$$

where b_{res} is the endogenous decay coefficient for active biomass (day⁻¹).

Electron-Donor Mass Balance

For the ED, we use a steady-state mass balance that includes utilization and molecular diffusion (Wanner et al., 2006).

$$0 = D_{\text{ED},f} \frac{\partial^2 S_d}{\partial z^2} - X_{f,a} q \quad (7)$$

$D_{\text{ED},f}$ is the diffusion constant for ED in the biofilm (cm² day⁻¹) and $X_{f,a}$ is the density of active biomass (mg-VS cm⁻³). We employ a no-flux boundary condition at the anode surface (Eq. (8)) and continuity of flux at the interface of the external diffusion layer with the outer surface of the biofilm (Eq. (9)):

$$0 = D_{\text{ED},f} \frac{\partial S_d}{\partial z} \Big|_{z=0} \quad (8)$$

$$D_{\text{ED},l} \frac{\partial S_d}{\partial z} \Big|_{z=L_f} = D_{\text{ED},f} \frac{\partial S_d}{\partial z} \Big|_{z=L_f} = \left(\frac{D_{\text{ED},l}}{L}\right) (S_{d,\text{bulk}} - S_{d,\text{surface}}) \quad (9)$$

$D_{\text{ED},l}$ (cm² day⁻¹) is the diffusion coefficient for ED in the bulk liquid, L is the thickness of the diffusion layer (cm), $S_{d,\text{bulk}}$ is the ED concentration in the bulk liquid (mmol-ED cm⁻³), and $S_{d,\text{surface}}$ is the ED concentration at the biofilm surface (mmol-ED cm⁻³).

Electron Balance And Ohm's Law

Typically, the mass balance on EA is described using a diffusion-utilization equation that looks like Eq. (7) (Wanner et al., 2006). For the biofilm anode, we describe electron conduction through the conductive biofilm matrix and to the anode based on an electron balance. The steady-state electron balance is:

$$0 = \frac{\partial j}{\partial z} + \frac{F\gamma_1}{\tau} f e^0 X_{f,a} q + \frac{F\gamma_2}{\tau} X_{f,a} r_{\text{res}} \quad (10)$$

where

j = current density (mA cm⁻²)

γ_1 = electron equivalence of ED (mmol-e⁻ mmol-ED⁻¹)

γ_2 = electron equivalence of active biomass (mmol-e⁻ mg-VS⁻¹) based on an empirical formula for microbial cells, $C_n H_a N_b O_c$; Rittmann and McCarty, 2001)

τ = time conversion (86,400 s day⁻¹)

$f e^0$ = fraction of electrons from the ED used for energy generation to support synthesis (dimensionless)

The first term on the right-hand side describes the change in current density or the flux of electrons in the conductive biofilm matrix. Electrons are generated from the oxidation of ED for the energy generation to fuel biomass synthesis

(second term) and the self-oxidation of biomass through endogenous respiration (third term).

We treat the biofilm matrix as a porous solid conductor according to Ohm's law (Bernardi and Verbrugge, 1991):

$$0 = \kappa_{\text{bio}} \frac{\partial \eta}{\partial z} + j \quad (11)$$

Eq. (11) states that a gradient in the local potential (i.e., the gradient in the activity of electrons) is required to drive current density (j). Similarity between Ohm's law and Fick's law of diffusion is noted by others (Palmer and Lindenberg, 1979), and the following analogies are apparent from Eq. (11): (1) biofilm conductivity and diffusion coefficient, (2) the gradient in the local potential and the gradient in chemical potential, and (3) current density and flux of chemical species. Eqs. (10) and (11) can be combined to give

$$0 = \kappa_{\text{bio}} \frac{\partial^2 \eta}{\partial z^2} - \frac{F\gamma_1}{\tau} f e^0 X_{f,a} q - \frac{F\gamma_2}{\tau} X_{f,a} r_{\text{res}} \quad (12)$$

which is analogous to the typical substrate mass balance equation for an EA. Eq. (12) requires two boundary conditions. The first is a fixed potential at the anode:

$$\eta|_{z=0} = V_{\text{anode}} \quad (13)$$

where V_{anode} is the anode voltage (V). A potentiostat can establish a poised anode potential experimentally (e.g., chronoamperometry). V_{anode} in this article is always defined relative to E_{K_A} . The second boundary condition is no electron flux at the diffusion-layer surface of the biofilm, since electrons do not conduct outside the biofilm matrix:

$$\left. \frac{\partial \eta}{\partial z} \right|_{z=L_f} = \frac{j|_{z=L_f}}{\kappa_{\text{bio}}} = 0 \quad (14)$$

Biomass Mass-Balance

We write the biomass mass-balance following the well-established framework for one-dimensional, multi-species biofilm model (Wanner and Gujer, 1986). In the multi-species framework, the volume fraction represents the fraction of space that each type of biomass occupies. We consider two types of biomass: active and inert. Inert biomass is a simple means to include conductive materials, including EPS and (if they are present) nanowires. The sum of the active and inert biomass volume fractions always adds up to one at all locations in biofilm.

$$1 = \phi_a + \phi_i \quad (15)$$

where ϕ_a and ϕ_i are the volume fraction of active or inert biomass, respectively. During dynamic simulations, the biofilm develops naturally into "fuzzy layers" (Kissel et al.,

1984; Rittmann and Manem, 1992; Wanner and Gujer, 1986) as the different types of biomass compete for space.

The following mass-balances for active and inert biomass state that the accumulation (first term on the left-hand side) and the advection of biomass (second term on the left-hand side) equal the growth, respiration, and decay of biomass (right-hand side) (Wanner and Gujer, 1986):

$$\frac{\partial \phi_a}{\partial t} + \frac{\partial(v\phi_a)}{\partial z} = Yq - r_{\text{res}} - r_{\text{ina}} \equiv \mu_a \quad (16)$$

$$\frac{\partial \phi_i}{\partial t} + \frac{\partial(v\phi_i)}{\partial z} = \frac{X_{f,a}}{X_{f,i}} r_{\text{ina}} \equiv \mu_i \quad (17)$$

where Y is the true yield ($\text{mg-VS mmol-ED}^{-1}$) and $X_{f,i}$ is the density of inert biomass (mg-VS cm^{-3}). The left-hand side of each equation describes the conservation of mass of each species due to accumulation and advection. Advection of biomass is characterized by the advective velocity of the biofilm matrix, v (cm day^{-1}). The right-hand side of each equation describes the net growth of each species and is defined by the net specific growth rate for the active (μ_a ; day^{-1}) and inert biomass (μ_i ; day^{-1}). The rate of inactivation of active biomass (r_{ina}) to form inert biomass is first-order in respect to ϕ_a :

$$r_{\text{ina}} = b_{\text{ina}} \phi_a \quad (18)$$

where b_{ina} (day^{-1}) is the first-order inactivation rate coefficient.

The advective velocity of the biofilm matrix changes in response to the net specific growth rates for active and inert biomass.

$$\frac{\partial v}{\partial z} = \mu_a + \mu_i \quad (19)$$

The advective velocity at any point, z' , in the biofilm can be determined by integrating the specific growth rate of the biofilm from the anode attachment surface to z' :

$$v(t, z') = \int_0^{z'} (\mu_a + \mu_i) dz \quad (20)$$

The thickness of the biofilm changes in response to the advective velocity of biomass and detachment of the biomass.

$$\frac{dL_f}{dt} = v(t, L_f) - b_{\text{det}} L_f \quad (21)$$

The second term is the loss of biomass due to detachment, with a first-order rate b_{det} (day^{-1}). We apply detachment only at the interface of the biofilm with the bulk-liquid to simulate erosion (Wanner et al., 2006).

Minimum Potential Required To Sustain A Steady-State Biofilm

In typical biofilm modeling, S_{\min} refers to the minimum substrate concentration required to sustain a steady-state biofilm. For single limitation by the acceptor substrate, $S_{\min} = S_{a,\min}$ is defined as (Rittmann and McCarty, 1980; Rittmann and McCarty, 2001):

$$S_{a,\min} = K_{S_a} \frac{b_{\text{ina}} + b_{\text{det}}}{(Yq_{\max} - b_{\text{res}}) - (b_{\text{ina}} + b_{\text{det}})} \quad (22)$$

An analog can be defined for the biofilm anode of an MFC. η_{\min} is the minimum local potential required to sustain a steady-state biofilm in the absence of ED limitation. Since η_{\min} is for the case of a minimal accumulation of biofilm, we ignore resistance to electron conduction in the biofilm. Then, the steady-state active-biomass mass balance can be rewritten as

$$\frac{Yq_{\max}X_{f,a}L_f}{1 + \exp\left(-\frac{F}{RT}\eta\right)} = X_{f,a}L_f(b_{\text{ina}} + b_{\text{det}}) + \frac{X_{f,a}L_f b_{\text{res}}}{1 + \exp\left(-\frac{F}{RT}\eta\right)} \quad (23)$$

The left-hand side is the rate of biomass synthesis and right-hand side gives the overall rate of biomass loss. Steady-state requires that $\eta \geq \eta_{\min}$, and Eq. (23) can be solved for the local potential to obtain $\eta_{\min} = \eta$:

$$\eta_{\min} = \frac{RT}{F} \ln\left(\frac{b_{\text{ina}} + b_{\text{det}}}{(Yq_{\max} - b_{\text{res}}) - (b_{\text{ina}} + b_{\text{det}})}\right) \quad (24)$$

While some details of Eq. (24) differ from Eq. (22), the form and the inherent meaning remain: the organisms must be provided enough potential so that the rate of biomass accumulation at least equals the rate of loss.

Figure 1 illustrates the relationship between η_{\min} and b_{det} for the standard conditions (described later), but with different Y values. In general, η_{\min} increases with b_{det} , approaching infinity as b_{det} approaches 0.2 and 0.5 day^{-1} , respectively, for the true yield values of 2.26 and 4.52 $\text{mg-VS mmol-Ac}^{-1}$. At a high detachment rate, the loss of biomass exceeds the rate of accumulation, and washout occurs; hence, steady-state biomass cannot be sustained at that detachment rate. For the largest yield, washout does not occur for b_{det} up to 0.6 day^{-1} . For all three yields, η_{\min} occurs between -0.2 and 0 V when not in washout. Thus, we explored $V_{\text{anode}} \geq 0$ V for all our dynamic growth models.

Stoichiometry Table

Table I summarizes the stoichiometric relationships among the four variables (ϕ_a , ϕ_i , S_d , and η) and the three kinetic processes (donor utilization, biomass inactivation, endo-

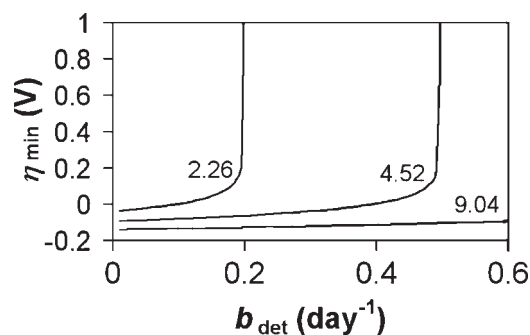


Figure 1. The relationship between η_{\min} and b_{det} as predicted by Eq. (24). The corresponding true yield value ($Y = 2.26, 4.52, \text{ or } 9.04$ as $\text{mg-VS mmol-Ac}^{-1}$) for each line is noted in the figure. Other parameters used for calculation are listed in Table II.

genous respiration) in the biofilm-anode model. Utilization of substrate produces active biomass and generates electrons that conduct. Active biomass is consumed by biomass inactivation and respiration. The inactivated biomass is converted into inert biomass, while the respired active biomass is converted into equivalent current. The conduction of electrons generated from substrate utilization and biomass respiration results in the change in local potential.

Solution Strategy

Substrate utilization, electron conduction, and substrate diffusion occur in the time scale of seconds or shorter, while the biological growth occurs over hours to days. The difference in time scales permits us to treat utilization, conduction, and diffusion as steady state for a series of “frozen states” for biomass (Kissel et al., 1984). For the biomass, we simplified the moving-interface problem by transforming the equations in the rescaled coordinate $\zeta \in [0,1]$, defined by $\zeta \equiv z/L_f$ (Wanner and Gujer, 1986). We used 50 grid points to represent the biofilm.

We adopted the following solution strategy:

1. Discretize Eqs. (7)–(9) and (12)–(14) by taking finite differences and obtain steady-state solution via Newton’s method (Chapra and Canale, 2001). This generates values of S_d and η in the biofilm.
2. Calculate the advective velocity of the biofilm matrix using Eq. (20).
3. Update the biofilm thickness (Eq. (21)) using only the growth term ($v(t, L_f)$).
4. For the solid-phase components, solve Eqs. (16) and (17) individually with a Backward-Euler step of 0.001 day. This generates new values for ϕ_a and ϕ_i .
5. Update the biofilm thickness (Eq. (21)) using only the detachment term, which removes biomass from the outer layer based on b_{det} and L_f .
6. Interpolate the remaining biomass onto a new grid and return to step 1.

Table I. Matrix of stoichiometry and kinetic expressions used for the MFC biofilm anode.

Process name	Biomass type		ED S_d	Potential η	Kinetic equation
	ϕ_a	ϕ_i			
ED utilization	Y		$-X_{f,a}$	$-\frac{F\gamma_1}{\tau} fe^0 X_{f,a}$	$q = q_{\max} \phi_a \frac{S_d}{S_d + K_{S_d}} \frac{1}{1 + \exp[-(F/RT)\eta]}$
Biomass inactivation	-1	$\frac{X_{f,a}}{X_{f,i}}$			$r_{ina} = b_{ina} \phi_a$
Biomass respiration	-1			$-\frac{F\gamma_2}{\tau} X_{f,a}$	$r_{res} = b_{res} \phi_a \frac{1}{1 + \exp[-(F/RT)\eta]}$

Model Parameters

The vertical coordinate in Figure 2 summarizes the relationships among potentials and voltages that we define for our model. We use the half-maximum-rate anodic-EA potential (E_{K_A}) as the reference potential; thus, $E_{K_A} \equiv 0$. The choice of E_{K_A} as the reference is appropriate because of its biological significance (i.e., half-maximum-rate). We define the anodic-EA potential (E_{anode}) as an analog of the EA concentration in traditional biofilm modeling. The value of E_{anode} changes along the depth of the biofilm, much like the EA concentration. The local potential (η) equals E_{anode} because we use E_{K_A} as the reference potential. However, η is always defined in reference to E_{K_A} , since $\eta = E_{anode} - E_{K_A}$.

We also define the anode voltage (V_{anode}), which is the voltage available to drive the processes at the anode. In an experimental MFC, V_{anode} equals the difference between E_{anode} at the anode surface (i.e., $E_{anode}|_{z=0}$) for an open cell (i.e., with zero current) and with current. These two E_{anode} potentials are typically measured against a standard reference electrode in an experimental MFC. Since E_{anode}

is defined with respect to E_{K_A} , we also define V_{anode} with respect to E_{K_A} ; thus, $V_{anode} = E_{anode}|_{z=0}$. Unlike E_{anode} , V_{anode} has no spatial dependence, but like E_{anode} , V_{anode} can be fixed using a potentiostat.

We estimate V_{anode} in our article using results from Bond and Lovley (2003), who poised the anode electrode potential at +0.2 V against the standard Ag/AgCl electrode while generating current. They measured an open-cell potential (i.e., no-current condition) of -0.42 V against the standard Ag/AgCl electrode. Thus, $V_{anode} = 0.2 - (-0.42) = 0.62$ V. E_{K_A} (half-maximum-rate) falls between -0.42 (i.e., zero current) and +0.2 (maximum current) V against the standard Ag/AgCl electrode. From the examination of the current-voltage curves (Liu et al., 2005), E_{K_A} of ~0.1 V above the OCP appears appropriate. Thus, we use $V_{anode} = 0.5$ V for our simulations.

Table II summarizes parameters common to all the model trials in this article. We estimated q_{\max} and K_{S_d} from bacteria known to catalyze oxidation reactions in a biofilm anode. The ED concentration in the bulk liquid was 3×10^{-4} mmol-Ac cm^{-3} unless specified otherwise; this corresponds to 19.2 mgBOD_L L^{-1} , typical for a wastewater treatment effluent. While the estimated parameters we used are useful in identifying the trends and conducting the analysis of the biofilm anode, we recognize that different MFC setting will have parameters unique to their biological, chemical, and physical conditions.

Parameter sets for the 18 model trials we performed are summarized in the left half of Table III. Since some pure-culture bacteria are able to transfer most of the electrons from the ED to the anode in respiration (Bond and Lovley, 2003), we compared two relatively high fe^0 values (0.9 and 0.95), where fe^0 is the fraction of ED electrons transferred to the EA for energy generation to support synthesis. The corresponding true yield values were 2.26 and 4.52 mg-VS mmol-Ac⁻¹. We used detachment rate coefficients of 0.05–0.2 day⁻¹ to compare the effects of detachment, biofilm conductivity of 1–10⁻⁵ mS cm^{-1} to study η limitation, and biofilm density of 40 or 200 mgVS cm^{-3} to represent moderately low and high biofilm densities, respectively. All results in the right-hand half of Table III were generated with $V_{anode} = 0.5$ V. We performed additional model trials using the parameters sets from Table III, but with different V_{anode} values (Fig. 3a) only).

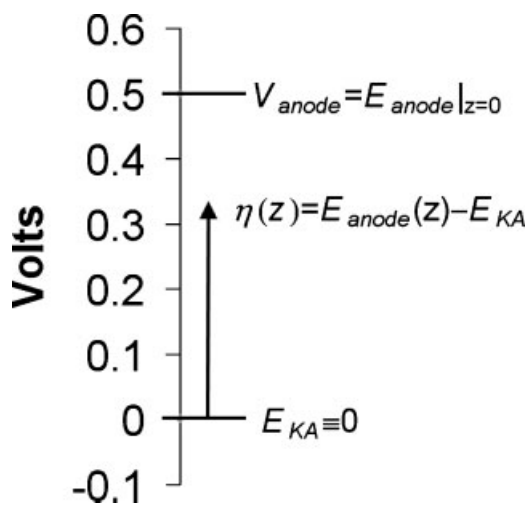


Figure 2. The vertical coordinate shows the relationships among potentials and voltages. E_{K_A} —half-maximum-rate anodic-acceptor potential (V); E_{anode} —anodic-electron-acceptor potential (V); η —local potential (V); and V_{anode} —anode voltage.

Table II. Common parameters for all trials.

Symbol	Description	Numerical values	Units	Reference
K_{S_d}	Half-max-rate acetate concentration	3×10^{-5a}	mmol cm^{-3}	Esteve-Nunez et al. (2005)
q_{\max}	Maximum specific rate of ED utilization	0.132	$\text{mmol-Ac mg-VS}^{-1} \text{day}^{-1}$	Calculated based on Bond and Lovley (2003) ^b
b_{ina}	Inactivation decay coefficient for active biomass	0.05 ^c	day^{-1}	assumed
b_{res}	Endogenous decay coefficient for active biomass	0.05 ^c	day^{-1}	assumed
L	Diffusion layer thickness	0.01 ^d	cm	assumed
$D_{\text{ED},l}$	Acetate diffusion coefficient	0.941	$\text{cm}^2 \text{day}^{-1}$	Lide (2006)
$D_{\text{ED},f}$	Acetate diffusion coefficient in biofilm	0.753	$\text{cm}^2 \text{day}^{-1}$	80% of $D_{\text{ED},l}$ ^e
γ_1	Electron equivalence of acetate	8	$\text{mmol-e}^- \text{mmol-Ac}^{-1}$	Calculated
γ_2	Electron equivalence of active biomass	0.177	$\text{mmol-e}^- \text{mgVS}^{-1}$	Assume $\text{C}_5\text{H}_7\text{O}_2\text{N}$ for VS
$S_{d,\text{bulk}}$	Bulk electron donor concentration	3×10^{-4}	mmol cm^{-3}	–

^aWe averaged values for K_{S_d} for *Geobacter sulfurreducens* utilizing acetate as the ED and two different electron acceptors: fumarate and iron citrate as electron acceptors.

^b*Geobacter sulfurreducens* catalyzing acetate oxidation at an anode, the maximum rate of acetate utilization observed was $1.2 \mu\text{mol-e}^- \mu\text{g-protein}^{-1} \text{min}^{-1}$ (Bond and Lovley, 2003). We made unit conversion assuming a protein content of about 55% (Whitman et al., 1998), $\text{C}_5\text{H}_7\text{O}_2\text{N}$ as the formula for cells grown with ammonium as the nitrogen source (Rittmann and McCarty, 2001) and cells are 90% volatile.

^cThe inactivation decay coefficients, b_{ina} and b_{res} , of 0.05 day^{-1} falls on the higher end for slow growing anaerobic bacteria (Rittmann and McCarty, 2001).

^dA typical value for the diffusion-layer thickness (Rittmann and McCarty, 2001).

^eCommonly the diffusion coefficient in the biofilm is about 80% of $D_{\text{ED},l}$ (Wanner et al., 2006).

Results and Discussion

We ran dynamic growth models for 250 and 400 days simulation time for the high and low Y values, respectively, to ensure steady state. We calculated a comparable current flux by converting the units of current density from A/m^2 to $\text{mmol-Ac cm}^{-2} \text{day}^{-1}$ using the Faraday constant and the electron equivalence of acetate ($8 \text{ e}^- \text{eq/mol-Ac}$). The right-

hand half of Table III summarizes the results for steady-state biofilm thickness, current density, ED flux, current flux, and Coulombic yield for the 18 trials with $V_{\text{anode}} = 0.5 \text{ V}$.

Table III reveals three trends. First, a decrease in the detachment rate (b_{det}) or an increase in the true yield (Y) results in an increase in the biofilm thickness. Good comparisons to show this trend are between Trials 1 and 2 (b_{det}) and Trials 1 and 8 (Y). Decreasing b_{det} by a factor of

Table III. Parameters and results for 18 model trials.

Symbols	Parameters					Results				
	$X_{f,a}$ and $X_{f,i}$	Y	f_e^0	κ_{bio}	b_{det}	L_f	Current density	ED flux	Current flux	Coulombic yield ^a
Units	mg-VS cm^{-3}	$\text{mg-VS mmol-Ac}^{-1}$	–	mS cm^{-1}	day^{-1}	μm	A m^{-2}	$\mu\text{mol-Ac cm}^{-2} \text{day}^{-1}$	$\mu\text{mol-Ac cm}^{-2} \text{day}^{-1}$	%
Trial 1	200	2.26	0.95	10^{-4}	0.05	23	1.08	12.6	12.1	96
Trial 2	↓	↓	↓	↓	0.1	12	1.11	12.9	12.4	96
Trial 3	↓	↓	↓	10^{-3}	0.05	33	1.98	22.9	22.2	97
Trial 4	↓	↓	↓	↓	0.1	18	1.82	21.0	20.3	96
Trial 5	↓	4.52	0.9	10^{-5}	0.05	19	0.39	4.8	4.3	91
Trial 6	↓	↓	↓	↓	0.1	9.8	0.39	4.8	4.3	91
Trial 7	↓	↓	↓	↓	0.2	4.9	0.39	4.8	4.4	91
Trial 8	↓	↓	↓	10^{-4}	0.05	53	1.08	13.4	12.2	91
Trial 9	↓	↓	↓	↓	0.1	28	1.14	14.0	12.8	91
Trial 10	↓	↓	↓	↓	0.2	15	1.17	14.4	13.1	91
Trial 11	↓	↓	↓	10^{-3}	0.05	64	1.66	20.0	18.5	93
Trial 12	↓	↓	↓	↓	0.1	39	1.94	23.4	21.7	93
Trial 13	↓	↓	↓	↓	0.2	22	1.92	23.4	21.5	92
Trial 14	40	↓	↓	↓	0.05	187	0.89	10.8	10.0	92
Trial 15	↓	↓	↓	↓	0.1	127	1.12	13.6	12.5	92
Trial 16	↓	↓	↓	↓	0.2	81	1.36	16.6	15.2	91
Trial 17 ^b	200	↓	↓	↓	0.2	53	4.2	51.5	46.7	91
Trial 18 ^b	↓	↓	↓	1	0.2	403	36	434	399	92

The left-hand half summarizes the parameter values used for each trial. The right-hand half summarizes the results generated with the parameter sets on the left-hand half with $V_{\text{anode}} = 0.5 \text{ V}$ after 400 or 250 days of simulation time, respectively, for Trials 1–4 and 5–18. We calculated the current flux by converting current density (A m^{-2}) to $\text{mmol-Ac cm}^{-2} \text{day}^{-1}$. The Coulombic yield is the ratio of the current flux divided by the ED flux.

^aCalculated as the ratio of the current flux divided by the ED flux.

^b10 mM of acetate in the bulk liquid.

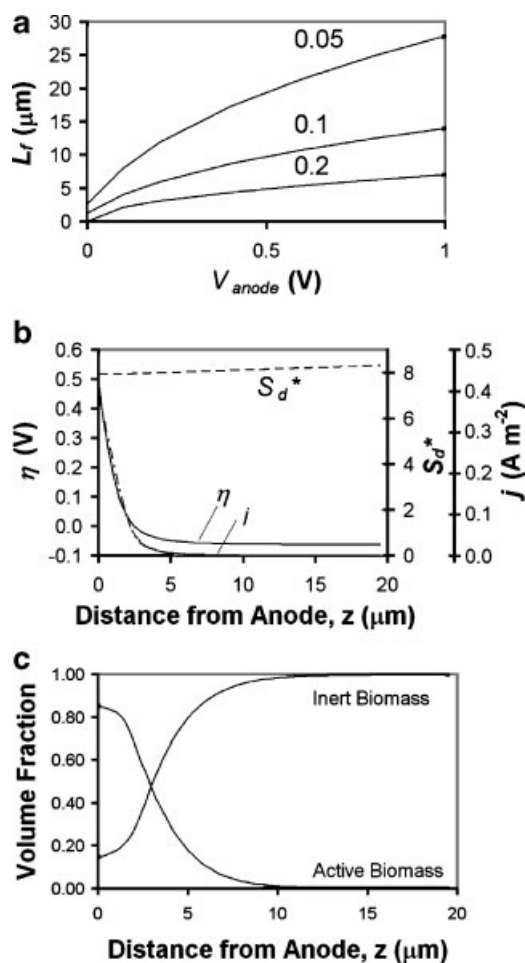


Figure 3. The simulation results for low conductivity biofilm ($\kappa_{\text{bio}} = 10^{-5}$ mS cm $^{-1}$). Trials 5, 6, and 7 (Table III) have b_{det} of 0.05, 0.1, and 0.2 day $^{-1}$, respectively. **a:** The relationship between the anode potential (V_{anode}) and steady-state biofilm thickness (L_f) established after 250 days. The corresponding b_{det} value is noted next to each line. **b:** The profile of the local potential (η), the dimensionless ED concentration (i.e., $S_d^* = S_d/K_{S_d}$) and the current density (j) along the depth of the biofilm after 250 days with $V_{\text{anode}} = 0.5$ V (Trial 5 only). **c:** The distribution of active and inert biomass along the depth of the biofilm after 250 days with $V_{\text{anode}} = 0.5$ V (Trial 5 only).

2 increases the biofilm thickness from 12 to 23 μm . Doubling Y increases the biofilm thickness from 23 to 53 μm . Second, the Coulombic yield (defined as the ratio of the ED current flux divided by the ED flux) is slightly greater than f_e^0 because the anode recovers electrons from ED and endogenous-biomass oxidations. For example, the Coulombic yield for Trial 1 is 96%, while f_e^0 is 95%. Coulombic yields from our Trials are in between 91% and 97%, which is in line 96.8% and 97% obtained in pure-culture studies (Bond and Lovley, 2003; Bond and Lovley, 2005). Third, the ED and current fluxes increase for all cases when κ_{bio} increases. A good example is between Trials 7 and 13. Increasing κ_{bio} from 10^{-5} to 10^{-3} mS cm $^{-1}$ increases the ED flux from 4.8 to 23.4 $\mu\text{mol-Ac cm}^{-2} \text{ day}^{-1}$ and the current flux from 4.4 to 21.5 $\mu\text{mol-Ac cm}^{-2} \text{ day}^{-1}$.

Figure 3 compares the dynamic simulation results for Trials 5–7 and additional simulations with different values of V_{anode} , all with a low biofilm conductivity of 10^{-5} mS cm $^{-1}$. Each line in Figure 3a shows the steady-state thickness established after 250 days and V_{anode} ranging from 0 to 1 V using the parameter sets from Trials 5–7. A decrease in b_{det} or an increase in V_{anode} results in a thicker biofilm. Despite the large differences in the steady-state biofilm thicknesses, the current densities produced from the three biofilms are almost identical for the anode potentials between 0.1 and 1 V (e.g., Table III for the 0.5-V result). This suggests that the biomass active in respiration in each biofilm is similar.

Figure 3b shows the profile of potential (η), the dimensionless ED concentration (i.e., $S_d^* = S_d/K_{S_d}$), and j (in A cm $^{-2}$) for Trial 5. We only show the profile for Trial 5 because its profile is nearly identical to Trials 6 and 7. Due to a low biofilm conductivity of 10^{-5} mS cm $^{-1}$, η rapidly falls below zero around $z = 2.5$ μm ; however, S_d^* is above 7.9 throughout the depth of biofilm. Thus, this biofilm is nearly fully penetrated with respect to S_d^* , but deep with respect to (and thus limited by) η for low conductance. Hence, the generation of current by active biomass is restricted to the first several μm from the biofilm anode.

The profiles of the biomass volume fraction for Trial 5 with $V_{\text{anode}} = 0.5$ V (Fig. 3c) shows that almost all active biomass is located within the first 10 μm from the anode, where the local potential is high enough to support net synthesis (Fig. 3b). For Trial 5, the potential required to support net synthesis (Eq. (24)) is $\eta_{\text{min}} = -0.088$ V. Net loss occurs around $z = 6.2$ μm as η approaches η_{min} . The active biomass beyond $z > 6.2$ μm occurs due to advection of active biomass grown near the anode surface, and inert biomass dominates the biofilm composition for $z > 3$ μm . A lower detachment rate allows the accumulation of extra inert biomass on the anode (Fig. 3a), but does not influence the ED utilization rate (Table III), since the rate is limited thoroughly by the local potential.

Figure 4 shows the simulation results for Trials 8–10, all with a medium biofilm conductivity of 10^{-4} mS cm $^{-1}$. Figure 4a and b show the dynamic biofilm growth for Trials 8–10. We only show $V_{\text{anode}} = 0.5$ V, because we observed similar trends at lower and higher values of V_{anode} . The biofilm thickness for the anode increases most rapidly for the lowest detachment rate of 0.05 day $^{-1}$ and more gradually for $b_{\text{det}} = 0.1$ and 0.2 day $^{-1}$ (Fig. 4a). The current density follows the same trend of rapid increase until the biofilm thickness reaches ~ 12 μm (Fig. 4b), when the current density peaks at 1.23 A m $^{-2}$. Then, the current density begins to decline. The decline is greatest for the lowest detachment rate, and the biofilm anode with a higher detachment rate ultimately produces more current: 1.17, 1.14, and 1.08 A m $^{-2}$, respectively, for the detachment rates of 0.2, 0.1, and 0.05 day $^{-1}$ (Table III).

Figure 4c shows the steady-state profiles for η and S_d^* along the depth of the biofilm anode for Trials 8–10 grown with $V_{\text{anode}} = 0.5$ V. Significant gradients in η and S_d^* are

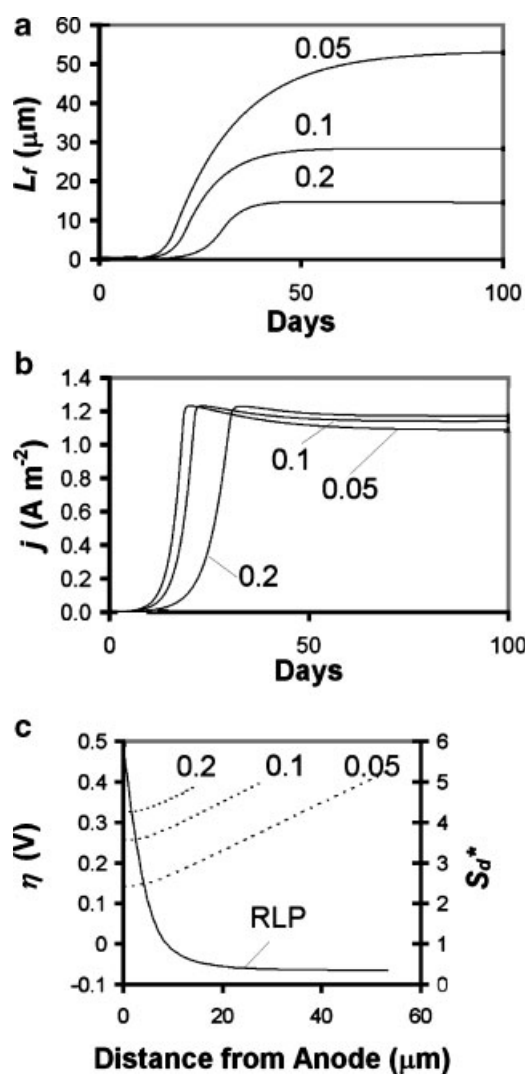


Figure 4. The simulation results for medium conductivity biofilm ($\kappa_{\text{bio}} = 10^{-4} \text{ mS cm}^{-1}$). Trials 8, 9, 10 (Table III) have b_{det} of 0.05, 0.1, and 0.2 day^{-1} , respectively, and the corresponding b_{det} value is noted for each line. $V_{\text{anode}} = 0.5 \text{ V}$. **a:** The change in the biofilm thickness (L_r) of the biofilm at different detachment rates. **b:** The change in the current density (j) of the biofilm anode at different detachment rates. **c:** The steady-state profile for the profile of the local potential (η) and the dimensionless ED concentration (S_d^*) for Trials 8–10 grown for 250 days. S_d^* is in dotted line. Since the local potential declines almost identically for $b_{\text{det}} = 0.05, 0.1, \text{ and } 0.2 \text{ day}^{-1}$, the line for $b_{\text{det}} = 0.05 \text{ day}^{-1}$ shows the representative local potential (RLP).

present for Trials 8–10. A tenfold increase in the biofilm conductivity from κ_{bio} from 10^{-5} to $10^{-4} \text{ mS cm}^{-1}$ increases the ED flux (Table III) and makes mass-transfer resistance significant. The profile of S_d^* changes significantly with b_{det} , while the profiles for η are nearly identical. The biofilm thickness increases from 15 to 53 μm for $b_{\text{det}} = 0.2$ and 0.05 day^{-1} (Fig. 4a). The thicker biofilm and the accumulation of inert biomass accentuate mass-transfer resistance and lower S_d^* near the anode, especially for Trial 8. The accumulated inert biomass physically separates the sources for η and S_d^* and accentuates dual limitation for the active biomass. This dual limitation effect leads to

decreases in current density (Fig. 4b), particularly for $b_{\text{det}} = 0.05 \text{ day}^{-1}$. Dual limitation is partially alleviated by removing excess biomass through increasing b_{det} . Fig. 4c illustrates that a higher b_{det} allows the active biomass to experience higher η and S_d^* simultaneously; hence, a higher detachment rates leads to a higher current density in the long term. For Trials 8–10, the optimal local potential and S_d^* occur with a biofilm thickness of $\sim 12 \mu\text{m}$, and the detachment rate of 0.2 day^{-1} keeps the steady-state biofilm near that optimal thickness. This example illustrates that removal, rather than the accumulation, of inert biomass is critical for the performance of the biofilm anode under a dual-limitation scenario.

Figure 5 shows the simulation results for Trials 11–13, all with a high biofilm conductivity of $10^{-3} \text{ mS cm}^{-1}$. Much like the medium-conductivity biofilm (Fig. 4b), removing excess inert biomass partially alleviates dual limitation, and the steady-state current density increases from 1.66 to 1.92 A m^{-2} as b_{det} increases from 0.05 to 0.2 day^{-1} (Fig. 5a). Figure 5b shows that η and S_d^* have significant gradients. Compared to Figure 4c, the gradient in η is shallow, but the gradient in S_d^* is steeper. Thus, the tenfold increase in biofilm conductivity makes the overall rate of electron transfer more limited by the donor substrate.

Figure 5c shows the distribution of active biomass when $\kappa_{\text{bio}} = 10^{-3} \text{ mS cm}^{-1}$. In contrast to low-conductivity biofilms (Fig. 3c), the active biomass can actively respire farther from the anode surface because high biofilm conductivity alleviates η limitation. Consequently, for $b_{\text{det}} = 0.05 \text{ day}^{-1}$, the greatest active biomass is localized around at 20–30 μm from the anode surface, where the limitations by S_d^* and η are at lowest (Fig. 5b and c). The removal of excess biomass minimizes η limitation (Fig. 5b), and the highest ϕ_a is found at the diffusion-layer surface of the biofilm for $b_{\text{det}} = 0.1$ and 0.2 day^{-1} (Fig. 5c). Furthermore, the slopes for the volume fractions of the active biomass become flat for the highest b_{det} because all biomass types experience similar conditions throughout the biofilm. Qualitatively, the biomass distribution under the high-conductivity scenario ($b_{\text{det}} = 0.2 \text{ day}^{-1}$, Fig. 5c) resembles the biomass distribution with *G. sulfurreducens* wild-type (Reguera et al., 2006).

Our model results illustrate that biomass detachment can be controlled as a means to improve the ED and current fluxes from the biofilm anode under a dual-limitation scenario. Especially when the conductivity is around $10^{-4} \text{ mS cm}^{-1}$, the current flux increases as b_{det} is increased (within the range we tested). A higher detachment rate is attained by creating an environment with stronger hydraulic shear force and turbulence, which also promotes a denser biofilm (Chang et al., 1991; Kwok et al., 1998). Thus, we compare biofilms with a high biofilm density of $200 \text{ mg-VS cm}^{-3}$ (Table III; Trials 11–13) and a low biofilm density of 40 mg-VS cm^{-3} (Table III; Trials 14–16). A decrease in the biofilm density increases the biofilm thickness (e.g., an increase from 64 to 187 μm for Trials 11 and 14), accentuating the effect of dual limitation by separating the diffusion layer and the anode (much like Fig. 4c). At the

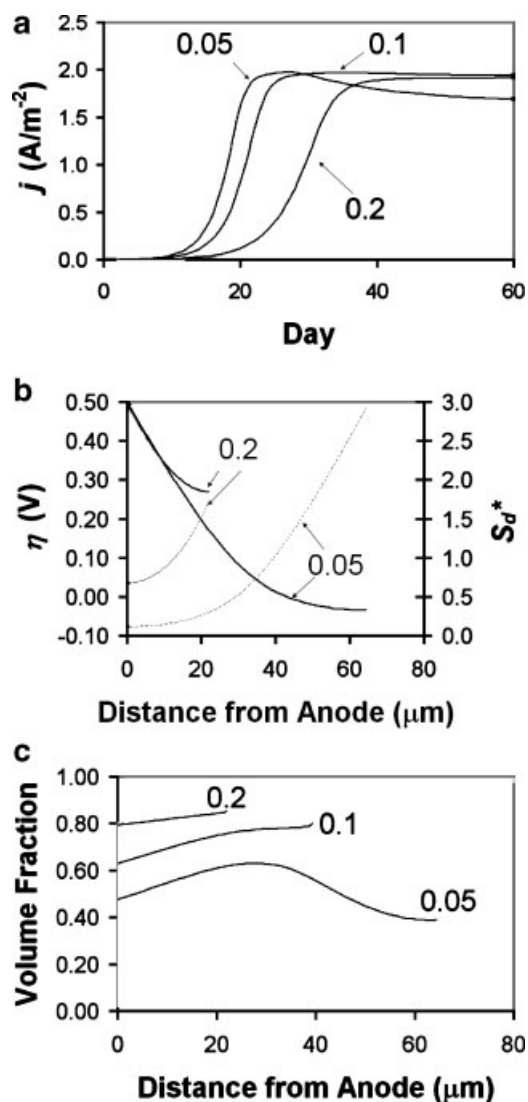


Figure 5. The simulation results for high conductivity biofilm ($\kappa_{\text{bio}} = 10^{-3}$ mS cm $^{-1}$). Trials 11, 12, and 13 have b_{det} of 0.05, 0.1, and 0.2 day $^{-1}$, respectively, and the corresponding b_{det} value is noted for each line. $V_{\text{anode}} = 0.5$. **a:** The change in the current density thickness (j) of the biofilm at different detachment rates. **b:** The steady-state profile for the local potential (η) and the dimensionless ED concentration (S_d^*) for Trials 11–13 grown for 250 day (the line for $b_{\text{det}} = 0.1$ day $^{-1}$ is omitted to improve the presentation). The solid line is η ; the dotted line is S_d^* . **c:** The steady-state profile for active biomass for Trials 11–13 grown for 250 days.

lowest detachment rate, $b_{\text{det}} = 0.05$, the high-density biofilm produces nearly twice as much current as the low-density biofilm (Trials 11 and 14). Thus, an environment with higher shear and turbulence may be favorable for the biofilm anode. While a high-turbulence environment is beneficial for the anode operation, promoting an environment with high shear and turbulence may incur an energy cost, a trade-off that must be investigated in the future.

For the dual-limitation scenarios (0.3 mM acetate in the bulk; Trials 1–16), the current density ranged from 0.39 to

1.94 A m $^{-2}$ with $\kappa_{\text{bio}} = 10^{-5}$ to 10^{-3} mS cm $^{-1}$. These values are in line with 0.16–1.14 A m $^{-2}$ obtained experimentally by Bond and Lovley (2003). Since Bond and Lovley conducted their experiments with as high as 10 mM of acetate, we ran Trial 17 with 10 mM of acetate in the bulk solution. An increase in the bulk acetate concentration from 0.3 to 10 mM (i.e., from Trial 13 to 17) increases the current density from 1.92 to 4.2 A m $^{-2}$ (Table III). Trial 17 has no ED limitation, as the ED concentration remains above 9 mM throughout the depth of the biofilm (not shown). Therefore, either $\kappa_{\text{bio}} = 10^{-3}$ mS cm $^{-1}$ is an overestimate for the biofilm of Bond and Lovley (2003) or factors other than the biofilm conductivity (e.g., pH gradients in biofilm) were limiting the current density. The reported maximum current density today is 8.2 A m $^{-2}$ with brush electrodes (Logan et al., 2007), and this suggests that κ_{bio} can be higher than 10^{-3} mS cm $^{-1}$. Increasing the biofilm conductivity from 10^{-3} to 1 mS cm $^{-1}$ (from Trial 17 to Trial 18) makes the biofilm solely limited by ED transport, and this increases the current density to 36 A m $^{-2}$ (now higher than observed by Logan et al., 2007). Based on this analysis, we expect that the actual conductivity of the biofilm anode is greater than 10^{-3} mS cm $^{-1}$, but probably significantly lower than 1 mS cm $^{-1}$.

Conclusion

In summary, we develop a dynamic, one-dimensional, multi-species model for the biofilm anode based on mass-balance principles, Ohm's law, and a novel Nernst-Monod expression to describe the rate of ED oxidation. The model describes that electrons from ED oxidation and endogenous respiration are electrically conducted from a bacterium, through the biofilm matrix, and into the anode. The parameter biofilm conductivity (κ_{bio}) describes the electrical conductivity of the biofilm anode.

We find that κ_{bio} strongly influences the ED and current fluxes, the type of limitation in biofilm and the biomass distribution. While the biofilm anode is limited by the electrical potential at a low $\kappa_{\text{bio}} = 10^{-5}$ mS cm $^{-1}$, ED mass-transfer resistance becomes significant at higher κ_{bio} . Consequently, the biofilm shifts from η limitation to dual limitation, and then to ED limitation as κ_{bio} increases from 10^{-5} to 10^{-3} mS cm $^{-1}$. Significant gradients for S_d^* , η , or both develop along the depth of the biofilm, and the active biomass fraction is high only where S_d^* and η are high. In particular, active biomass persists away from the anode as κ_{bio} increases.

The effects of dual limitation are accentuated by increases in biofilm thickness and accumulation of inert biomass. An increase in the biofilm detachment rate, the biofilm density, or both alleviates the dual-limitation effects by reducing biofilm thickness and removing excess inert biomass; the biofilm anode produces more current density in the long run when the biofilm thickness is not too great. An environment with higher shear and turbulence, which promotes a high

specific detachment rate and biofilm density, may be favorable for the biofilm anode.

We thank Dr. Richard Lueptow for the initial start up effort, Brian Merkey for insightful discussions, and Kyla Anderson for her administrative assistance.

References

- Bae W, Rittmann BE. 1996. Responses of intracellular cofactors to single and dual substrate limitations. *Biotechnol Bioeng* 49:690–699.
- Bae W, Rittmann BE. 1996. A structured model of dual-limitation kinetics. *Biotechnol Bioeng* 49:683–689.
- Bard AJ, Faulkner LR. 2001. *Electrochemical methods: Fundamentals and applications*. 2nd edn. New York: John Wiley.
- Bernardi DM, Verbrugge MW. 1991. Mathematical-model of a gas-diffusion electrode bonded to a polymer electrolyte. *AIChE J* 37: 1151–1163.
- Bernardi DM, Verbrugge MW. 1992. A mathematical-model of the solid-polymer-electrolyte fuel-cell. *J Electrochem Soc* 139:2477–2491.
- Bond DR, Holmes DE, Tender LM, Lovley DR. 2002. Electrode-reducing microorganisms that harvest energy from marine sediments. *Science* 295:483–485.
- Bond DR, Lovley DR. 2003. Electricity production by *Geobacter sulfurreducens* attached to electrodes. *Appl Environ Microbiol* 69:1548–1555.
- Bond DR, Lovley DR. 2005. Evidence for involvement of an electron shuttle in electricity generation by *Geothrix fermentans*. *Appl Environ Microbiol* 71:2186–2189.
- Chang HT, Rittmann BE, Amar D, Heim R, Ehlinger O, Lesty Y. 1991. Biofilm detachment mechanisms in a liquid-fluidized bed. *Biotechnol Bioeng* 38:499–506.
- Chapra SC, Canale RP. 2001. *Numerical methods for engineers: With software and programming applications*. 4th edn. Boston: McGraw-Hill.
- Dignac MF, Urbain V, Rybacki D, Bruchet A, Snidaro D, Scribe P. 1998. Chemical description of extracellular polymers: Implication on activated sludge floc structure. *Water Sci Technol* 38:45–53.
- Eddowes MJ, Hill HAO. 1977. Novel method for investigation of electrochemistry of metalloproteins—cytochrome-C. *J Chem Soc Chem Comm* 771–772.
- Esteve-Nunez A, Rothermich M, Sharma M, Lovley D. 2005. Growth of *Geobacter sulfurreducens* under nutrient-limiting conditions in continuous culture. *Environ Microbiol* 7:641–648.
- Gil GC, Chang IS, Kim BH, Kim M, Jang JK, Park HS, Kim HJ. 2003. Operational parameters affecting the performance of a mediator-less microbial fuel cell. *Biosens Bioelectron* 18:327–334.
- Gorby YA, Yanina S, McLean JS, Rosso KM, Moyles D, Dohnalkova A, Beveridge TJ, Chang IS, Kim BH, Kim KS, Culley DE, Reed SB, Romine MF, Saffarini DA, Hill EA, Shi L, Elias DA, Kennedy DW, Pinchuk G, Watanabe K, Ishii S, Logan B, Nealon KH, Fredrickson JK. 2006. Electrically conductive bacterial nanowires produced by *Shewanella oneidensis* strain MR-1 and other microorganisms. *Proc Natl Acad Sci USA* 103:11358–11363.
- Holmes DE, Bond DR, Lovley DR. 2004. Electron transfer by *Desulfobulbus propionicus* to Fe (III) and graphite electrodes. *Appl Environ Microbiol* 70:1234–1237.
- Kim BH, Chang IS, Gil GC, Park HS, Kim HJ. 2003. Novel BOD (biological oxygen demand) sensor using mediator-less microbial fuel cell. *Biotechnol Lett* 25:541–545.
- Kim BH, Park HS, Kim HJ, Kim GT, Chang IS, Lee J, Phung NT. 2004. Enrichment of microbial community generating electricity using a fuel-cell-type electrochemical cell. *Appl Microbiol Biotechnol* 63:672–681.
- Kissel JC, McCarty PL, Street RL. 1984. Numerical-simulation of mixed-culture biofilm. *J Environ Eng-Asce* 110:393–411.
- Kwok WK, Picioreanu C, Ong SL, van Loosdrecht MCM, Ng WJ, Heijnen JJ. 1998. Influence of biomass production and detachment forces on biofilm structures in a biofilm airlift suspension reactor. *Biotechnol Bioeng* 58:400–407.
- Laspidou CS, Rittmann BE. 2004. Modeling the development of biofilm density including active bacteria, inert biomass, and extracellular polymeric substances. *Water Res* 38:3349–3361.
- Lee JY, Phung NT, Chang IS, Kim BH, Sung HC. 2003. Use of acetate for enrichment of electrochemically active microorganisms and their 16S rDNA analyses. *Fems Microbiol Lett* 223:185–191.
- Lide DR. 2006. *CRC handbook of chemistry and physics*. 87th, 2006–2007 edn. Cleveland: CRC Press.
- Liu H, Cheng SA, Logan BE. 2005. Production of electricity from acetate or butyrate using a single-chamber microbial fuel cell. *Environ Sci Technol* 39:658–662.
- Liu H, Logan BE. 2004. Electricity generation using an air-cathode single chamber microbial fuel cell in the presence and absence of a proton exchange membrane. *Environ Sci Technol* 38:4040–4046.
- Logan BE, Cheng S, Watson V, Estadt G. 2007. Graphite fiber brush anodes for increased power production in air-cathode microbial fuel cells. *Environ Sci Technol* 41(9):3341–3346.
- Nielsen PH, Jahn A, Palmgren R. 1997. Conceptual model for production and composition of exopolymers in biofilms. *Water Sci Technol* 36: 11–19.
- Palmes ED, Lindenboom RH. 1979. Ohms law, Ficks law, and diffusion samplers for gases. *Anal Chem* 51:2400–2401.
- Rabaey K, Boon N, Hofte M, Verstraete W. 2005. Microbial phenazine production enhances electron transfer in biofuel cells. *Environ Sci Technol* 39:3401–3408.
- Reguera G, Nevin KP, Nicoll JS, Covalla SF, Woodard TL, Lovley DR. 2006. Biofilm and nanowire production leads to increased current in *Geobacter sulfurreducens* fuel cells. *Appl Environ Microbiol* 72:7345–7348.
- Rittmann BE, Manem JA. 1992. Development and experimental evaluation of a steady-state, multispecies biofilm model. *Biotechnol Bioeng* 39:914–922.
- Rittmann BE, McCarty PL. 1980. Model of steady-state-biofilm kinetics. *Biotechnol Bioeng* 22:2343–2357.
- Rittmann BE, McCarty PL. 2001. *Environmental biotechnology: Principles and applications*. New York: McGraw-Hill.
- Stumm W, Morgan JJ. 1996. *Aquatic chemistry: Chemical equilibria and rates in natural waters*. 3rd edn. New York: John Wiley.
- Ter Heijne A, Hamelers HVM, De Wilde V, Rozendal RA, Buisman CJN. 2006. A bipolar membrane combined with ferric iron reduction as an efficient cathode system in microbial fuel cells. *Environ Sci Technol* 40: 5200–5205.
- Wang J. 2000. *Analytical electrochemistry*. 2nd edn. New York: John Wiley.
- Wanner O, Ebert HJ, Morgenroth E, Noguera D, Picioreanu C, Rittmann BE, Van Loosdrecht MCM. 2006. *Mathematical modeling of biofilms*. IWA Scientific and Technical Report No.18 IWA Task Group on Biofilm Modeling.
- Wanner O, Gujer W. 1986. A multispecies biofilm model. *Biotechnol Bioeng* 28:314–328.
- Whitman WB, Coleman DC, Wiebe WJ. 1998. Prokaryotes: The unseen majority. *Proc Natl Acad Sci USA* 95:6578–6583.
- Yeh P, Kuwana T. 1977. Reversible electrode-reaction of cytochrome-C. *Chem Lett* 1145–1148.